A EUROPEAN JOURNAL

CHEMPHYSCHEM

OF CHEMICAL PHYSICS AND PHYSICAL CHEMISTRY

Accepted Article

Title: Hydrogen generating Ru/Pt bimetallic photocatalysts based on phenyl-phenanthroline peripheral ligands

Authors: Laura O'Reilly, Qing Pan, Nivedita Das, Kasper Wenderich, Jeroen Korterik, Johannes Vos, Dr. Mary Pryce, and Annemarie Huijser

To be cited as: *ChemPhysChem* 10.1002/cphc.201800658

Link to VoR: http://dx.doi.org/10.1002/cphc.201800658

A Journal of ChemPubSoc Europe

WILEY-VCH www.chemphyschem.org

WILEY-VCH

ARTICLE

Hydrogen generating Ru/Pt bimetallic photocatalysts based on phenyl-phenanthroline peripheral ligands

Laura O'Reilly,[a] Qing Pan,[b] Nivedita Das,[a] Kasper Wenderich,[b] Jeroen P. Korterik,[b] Johannes G. Vos,[a] Mary T. Pryce*[a] and Annemarie Huijser*[b]

Abstract Recent studies on hydrogen generating supramolecular bimetallic photocatalysts indicate a more important role of the peripheral ligands than expected, motivating us to design a Ru/Pt complex with 4,7-diphenyl-1,10-phenanthroline peripheral ligands. Photoinduced intra- and inter-ligand internal conversion processes have been investigated using transient absorption spectroscopy, spanning the femto- to nanosecond timescale. After photoexcitation and ultrafast intersystem crossing, triplet states localised on either the peripheral ligands or on the bridging ligand/catalytic unit are populated in a non-equilibrated way. Time-resolved photoluminescence demonstrates that the lifetime for the Ru/Pt dinuclear species (795±8 ns) is significantly less than that of the mononuclear analogue (1375±20 ns). The photocatalytic studies show modest hydrogen turnover numbers, which is possibly caused by the absence of an excited state equilibrium. Finally, we identify challenges that must be overcome to further develop this class of photocatalysts and propose directions for future research.

Introduction

The transition from fossil fuels to renewable energy is one of the most important challenges currently facing society. Solar devices are widely considered as highly promising, as energy provided by the sun to the earth far exceeds global needs.[1] A key limitation of photovoltaic cells and other renewable energy conversion systems such as wind and tidal energy is the lack of effective storage options and this drives research towards the development of solar-to-fuel devices. The insights obtained from extensive studies on photosynthetic light-harvesting complexes are inspiring the development of biomimetic systems capable of producing solar fuels such as hydrogen.[3] Within this framework, Ru^{II}-polypyridyl complexes are attracting wide interest, in large part due to their strong visible light absorption, ultrafast intersystem crossing, long excited state lifetimes and excellent redox reversibility.[4]

Two distinct strategies can be adopted to realise homogeneous photocatalytic proton reduction into H_2. The inter-molecular approach is based on the use of a mixture containing both photosensitiser and catalyst components[3a,b] and a sacrificial agent to regenerate the photosensitiser after light-induced electron transfer to the catalyst has taken place. A drawback of this strategy is that electron transfer between the individual components is diffusion limited. This has motivated the intra-molecular approach, based on supramolecular photocatalysts containing a photosensitiser as well as a catalytic moiety (Fig. 1).

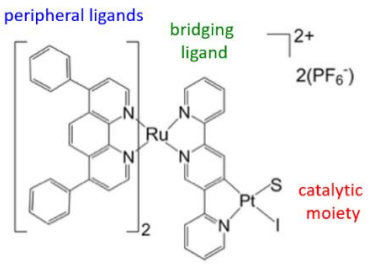

Figure 1. Chemical structure of **$RuPt_{dpph}$**. The mononuclear Ru^{II}-precursor is denoted as **Ru_{dpph}**, S = solvent.

Ru-polypyridyl complexes are widely selected as the photosensitiser, while Pt- or Pd-based moieties bound via a bridging ligand are attractive catalytic centers due to their low overpotential for proton reduction.[5] As proton reduction into H_2 generation requires the accumulation of two electrons at the catalyst, the common design strategy is based on the bridging ligand functioning as an electron storage reservoir for the first photo-excited electron.[6] The reactivity of such assemblies depends on the structure of the individual components.[7] Ideally, light-induced electron transfer from the photosensitiser via the bridging ligand to the catalyst should occur with a high quantum yield for efficient H_2 generation. However, this is not always the case. We have recently observed for a series of Ru/Pd and Ru/Pt photocatalysts that photoexcitation not only leads to population of Franck-Condon states localised on the bridging ligand, but also of states localised on the peripheral ligands.[8] A similar effect has been observed by others for a related Ru/Pd complex.[9] Efficient inter-ligand electron transfer (ILET) from the peripheral ligands to the bridging ligand is essential in these cases and needs to outperform other ultrafast decay pathways at the peripheral ligands such as vibrational relaxation which usually occurs over 5-15 ps.[8b, 10]

Photophysical studies have shown that ILET can occur over a wide time range, ranging from ps to sub-ns timescales.[8b, 11] Sakai *et al.* have tuned the driving force for ILET in a Ru/Pt complex by functionalising the bridging ligand with various functional groups. Relative to the COOH analogue, the CN functionalised photocatalyst shows an almost 6-fold increase in the ILET rate ($1.78 \cdot 10^{10}$ s^{-1}, i.e. *ca.* 56 ps) and a 3-fold improvement in initial H_2 generation reactivity, highlighting the

[a] L. O'Reilly, Dr. N. Das, Prof. J.G. Vos, Dr. M.T. Pryce
SRC for Solar Energy Conversion, School of Chemical Sciences
Dublin City University
Glasnevin, Dublin 9 (Ireland).
E-mail: mary.pryce@dcu.ie
[b] Dr. Q. Pan, Dr. K. Wenderich, J.P. Korterik, Dr. A. Huijser
Photocatalytic Synthesis and Optical Sciences groups
MESA+ Institute for Nanotechnology, University of Twente
P.O. Box 217, 7500 AE, Enschede (The Netherlands).
E-mail: j.m.huijser@utwente.nl

Supporting information for this article is given via a link at the end of the document.

importance of fast ILET to the bridging ligand. However, for both complexes it has been observed that 30-40 % of the excited states decay within *ca.* 1 ps, thereby limiting the photocatalytic performance.[11c] This fast decay may be caused by the close proximity of the bridging ligand to the catalytic moiety due to more efficient radiative decay caused by spin-orbit coupling and/or other intra-molecular non-radiative excited state decay channels.[8b,12] Such effects may explain the lower photoluminescence lifetime often observed for Ru/Pt and Ru/Pd complexes relative to their mononuclear Ru^{II} precursors.[7a, 8a] Also the crucial electron transfer step from the bridging ligand to the catalyst likely plays a role in the observed reduction in photoluminescence lifetime.

The use of the peripheral ligands instead of the bridging ligand as the electron storage reservoir may provide an opportunity to tune the tradeoff between fast ILET and a long excited state lifetime.[13] We have recently realised a substantial improvement in photocatalytic efficiency by functionalising peripheral ligands with electron withdrawing ester substituents (complex **$RuPt_{dceb}$**, dceb = 4,4-di(carboxyethyl)bipyridine, see Table 1), resulting in H_2 turn-over number (TON) and turn-over frequency (TOF) values amongst the highest reported to date for a supramolecular Ru/Pt photocatalyst.[14] Studies from Brewer and colleagues have shown that altering the peripheral ligand (PL) in $[\{(PL)_2Ru(dpp)\}_2RhBr_2]^{5+}$ assemblies (dpp = 2,3-bis (2-pyridyl)pyrazine, PL = 1,10-phenanthroline (phen), 2,2'-bipyridine (bpy) or 4,7-diphenyl-1,10-phenanthroline (dpph) can have a significant effect on the quantity of H_2 observed.[15] For these Ru-Rh assemblies, TONs (5 h irradiation by a 470 nm LED) for photocatalytic H_2 generation were in the order phen (20) < bpy (31) < dpph (140). The increased levels of H_2 generation with the introduction of dpph have been attributed to the steric demands of this peripheral ligand, thereby protecting the reduced catalytic species from other side reactions. The choice of peripheral ligands could also affect the photocatalytic H_2 production by influencing the visible light absorption.[7e] In addition to altering the excited state lifetime, the position of the electron storage reservoir may also affect accumulative charge separation.[16] Although probing the second photogenerated electron is challenging, electrochemical reduction of the bridging ligand has been found to impair transfer of the photo-generated electron (mimicking the second electron) towards the bridging ligand.[17]

These studies, which highlight an unexpected important role for the peripheral ligands, have motivated us to develop a novel **$RuPt_{dpph}$** photocatalyst (Fig. 1) incorporating dpph as peripheral ligands. These ligands were introduced since they may lead to long-lived triplet metal-to-ligand charge transfer (^{3}MLCT) states.[18] **$RuPt_{dpph}$** is based on a 2,2':5',2''-terpyridine (tpy) bridging ligand, which generally outperforms alternatives like 2,2':6',2''-terpyridine[7a], 2,3-di(pyridine-2-yl)pyrazine[8a] and 2,5-di(pyridine-2-yl)pyrazine[7b, 19] in terms of accessibility of the deactivating Ru^{II} metal-centered state and capability to accept electron density from the peripheral ligands.[8b] The structure of the catalytic moiety is motivated by recent work by Rau *et al.* indicating a superior photocatalytic reactivity and stability for photocatalysts based on a Pt iodide moiety compared to the Pt chloride or Pd chloride equivalents.[7c, 7d] Our recent work on the analogous **$RuPt_{bpy}$** compound has shown that the coupling between the tpy bridging ligand and the Pt iodide moiety likely induces a lower-lying triplet state (denoted as T_3), which quenches populated ^{3}MLCT states on a ~1 ps timescale. This T_3 state may involve electron density delocalisation over the tpy-Pt-I moiety via a backbonding effect.[20] An important question is whether a similar quenching process also occurs in **$RuPt_{dpph}$**.

The present study focuses on the impact that replacing the peripheral bpy ligands with dpph has on the early-time photodynamics, the excited state lifetime and the H_2 generating performance. Although side reactions prevent photophysical studies under catalytic conditions, earlier studies have shown that the photodynamics under non-catalytic conditions provide important mechanistic insight into the photocatalytic performance.[11c, 21] Even though H_2 formation likely occurs at a relatively slow timescale, the initial electron density distribution of the excited states populated by photoexcitation has been found to determine the H_2 generation efficiency.[9] Hence, understanding the role of the chemical structure in the early-time photodynamics is an important first step towards the design of efficient photocatalysts. In addition, insight into the nature of intermediate species[11c, 22] and inter-molecular interactions[19] is essential.

Results and Discussion

Figure 2a shows the steady-state absorbance and photoluminescence spectra of **$RuPt_{dpph}$** and its mononuclear Ru^{II}-precursor **Ru_{dpph}**. As expected for Ru^{II}-polypyridyl complexes, **Ru_{dpph}** shows a broad singlet ligand-to-metal charge transfer (^{1}MLCT) absorption band from *ca.* 380 nm - 550 nm.[4a] [7e] On the basis of earlier work on a related Ru^{II}-tpy complex[8b], the shoulder around 315 nm is assigned to a tpy ligand-centered π-π* transition. The sharp band centered at 278 nm is ascribed to a dpph ligand-centered π-π* transition, in agreement with earlier work by Brewer and colleagues.[7e] The ^{1}MLCT absorption band of **$RuPt_{dpph}$** is redshifted by ~8 nm relative to **Ru_{dpph}**, indicating that cyclometallation with the Pt moiety only marginally modifies the electronic levels of the ground and/or excited states. In addition to Ru-based ^{1}MLCT transitions, Ru/Pt complexes are also known for Pt-based ^{1}MLCT transitions, in particular in the range between 300-420 nm.[25] The photoluminescence reflects the decay of the lowest ^{3}MLCT states to the ground state, with a redshift in the maximum emission from 627 nm for **Ru_{dpph}** to 646 nm for **$RuPt_{dpph}$**, indicating that the Pt moiety induces a minor reduction in the energy gap between the excited and ground states. The photoluminescence quantum yield of **$RuPt_{dpph}$** is significantly lower compared to **Ru_{dpph}**, indicating a reduction in the photoluminescence rate constant and/or increase in rate(s) of competing non-radiative decay pathways. Table 1 compares the absorbance and photoluminescence properties and the H_2 TOF and TON values of **$RuPt_{dpph}$** with **Ru_{dpph}**, **$RuPt_{bpy}$** and **$RuPt_{dceb}$**.[14] Substitution of bpy by dpph peripheral ligands does not substantially affect the steady-state optical properties, therefore suggesting that the transient absorption bands of **$RuPt_{dpph}$** discussed below are comparable to those of **$RuPt_{bpy}$**.

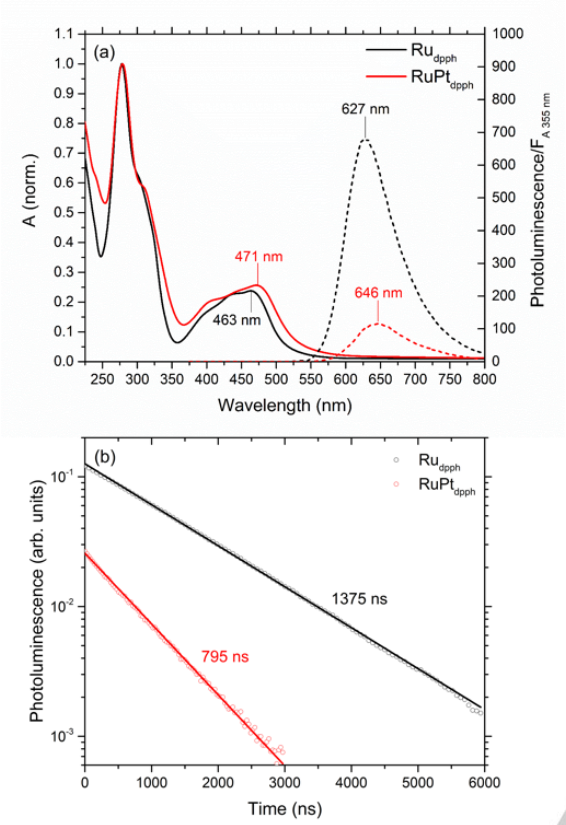

Figure 2. (a) Steady-state absorbance and photoluminescence spectra and (b) photoluminescence decays at the maximum emission of **Ru$_{dpph}$** and **RuPt$_{dpph}$** in anhydrous acetonitrile. Fits to a mono-exponential decay function are included as solid lines.

Table 1. Absorbance, photoluminescence and H_2 generating properties of the complexes discussed. In all cases tpy is used as bridging ligand. The Ru/Pt complexes are based on a Pt-I catalytic moiety.

	π-π* abs. λ_{max} (nm) peripheral ligands	π-π* abs. λ_{max} (nm) tpy bridging ligand	^{1}MLCT abs. λ_{max} (nm)	Emission λ_{max} (nm)/lifetime (ns, (%))	TOF (h^{-1}) / TON (after 6 h)
Ru$_{dpph}$	278	~315	464	627/1375 (100)	8/26
RuPt$_{dpph}$	~240 280	~315	471	646/795 (100)	24/54
RuPt$_{bpy}$[14]	~240 287	~320	457	645/136(12); 659(88)	15/80
RuPt$_{dceb}$[14]	246 ~311	~311	483	662/624 (100)	200/650

[a] The photocatalytic experiments were performed in a mixture of 60 vol% acetonitrile, 10 vol% water and 30 vol% triethylamine (TEA), at 470 nm irradiation and under a N_2 atmosphere.

The photocatalytic H_2 generating reactivity of **RuPt$_{dpph}$** has been measured using triethylamine (TEA) as a sacrificial agent, in similar reaction conditions to previous studies using **RuPt$_{bpy}$**.[14] No H_2 generation was observed in the dark, whereas upon irradiation at 470 nm modest TONs of 54 were obtained for **RuPt$_{dpph}$** after 6 h (see Fig. 3). In comparison to **Ru$_{dpph}$** mixed in solution with the Pt catalyst and TEA (*i.e.* the inter-molecular approach), **RuPt$_{dpph}$** is superior with a doubling in the amount of H_2 produced. The initial H_2 TOF of **RuPt$_{dpph}$** of 24 h^{-1} outperforms **RuPt$_{bpy}$** (TOF = 15 h^{-1}).[14] The initial H_2 TOF of **RuPt$_{dpph}$** is however lower than the value obtained for **RuPt$_{dceb}$**[14], despite the longer photoluminescence lifetime (see Table 1). The possible reasons will be discussed below. The stability of **RuPt$_{dpph}$** is limited to *ca.* 2 h, which may be due to the presence of the sacrificial agent. Improving the stability is a key challenge in solution based studies with sacrificial agents.

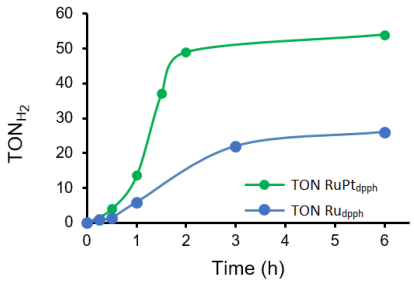

Figure 3. Photocatalysis results following irradiation at 470 nm of both **Ru$_{dpph}$** and **RuPt$_{dpph}$** in 60% acetonitrile, 10% water and 30% TEA (concentration of **Ru$_{dpph}$**/($Pt(CH_3CN)_2I_2$) or **RuPt$_{dpph}$** ~$1.7x10^{-5}$ M). The **Ru$_{dpph}$** complex is mixed with an equimolar amount of Pt catalyst (*i.e.* the inter-molecular approach).

To understand why the promising long ^{3}MLCT lifetimes observed by time-resolved photoluminescence result in modest photocatalytic performance, early-time excited state processes have been characterised by fs transient absorption (TA). Figure 4a shows the TA spectra of **Ru$_{dpph}$** at various time delays, measured using an excitation wavelength (λ_{exc}) of 490 nm. As intersystem crossing in these complexes is likely to occur within 100 fs,[4b, 4c, 23] the spectra are assigned to triplet rather than singlet excited states. The negative signal between 430 nm and 500 nm overlaps with the scaled and inverted steady-state absorbance spectrum (included as grey area) and is assigned to ground state bleach (GSB). In addition, three excited state absorption (ESA) regions can be distinguished. The broad ESA band >500 nm is likely due to ligand-to-metal charge transfer transitions,[8b,10b] probably with both contributions from reduced tpy[8b] and dpph[11b] ligands. A second broad ESA band centered at ~420 nm and partially overlapping with the GSB is likely due to ligand-centered transitions of the reduced tpy ligand, in agreement with earlier assignments.[8b, 20] The significantly weaker ~5 ps rise of the ESA signal probed at 360 nm compared to *e.g.* 395 nm (see Fig. 4c) suggests a third ESA band, likely due to ligand-centered transitions of the reduced dpph ligands. These transitions have been reported to be blue-shifted[24] relative to analoguous transitions for bpy ligands typically observed around 370 nm.[8b, 20] These ESA signals indicate that, similar to **RuPt$_{bpy}$** and its mononuclear precursor **Ru$_{bpy}$**[8b, 20], both ^{3}MLCT states localised on the peripheral ligands and states localised on the bridging ligand are populated after ultrafast intersystem crossing.

To determine if the population of the $^3MLCT_{tpy}$ and $^3MLCT_{dpph}$ states is equilibrated, TA experiments have also been performed using 515 nm excitation (Fig. 4b). The spectrotemporal behavior shown in Figures 4a and 4b is comparable. However, global analysis of all TA data using a one-component sequential model[2] (the solid lines in Figs. 4a-d present the achieved fit) and the obtained evolution associated spectra (EAS, Fig. 6a) suggest a modest role of the photoexcitation wavelength. The shape of the broad and featureless ESA band >500 nm likely due to both reduced tpy[8b] and dpph ligands[11b] has changed. Experiments at longer wavelengths to verify this effect were however not performed due to the low absorbance of the compound in this region.

The kinetic traces shown in Figures 4c (λ_{exc} = 490 nm) and 4d (λ_{exc} = 515 nm) illustrate the temporal evolution of the TA bands observed. The GSB band centered around 460 nm develops in the instrumental response time of *ca.* 100 fs and then remains constant, showing that any excited state decay is insignificant in the sub-ns experimental time window, in agreement with the 1375±20 ns photoluminescence lifetime (Fig. 2b). The ESA signal at 395 nm (and to a lower extent the signal at 360 nm) clearly shows a ~5 ps rise, indicating an increase in population of $^3MLCT_{tpy}$ states, and stabilizes in *ca.* 20 ps.

The low number of probe photons generated by the CaF_2 crystal in the UV (and especially below 360 nm) resulting in a poor S/N ratio does not allow us to observe a simultaneous decrease of a potential ESA band below *ca.* 350 nm associated to the population of the $^3MLCT_{dpph}$ states (possibly contributing to the ESA signal at 360 nm, in addition to $^3MLCT_{tpy}$ states). Global analysis based on a one-component sequential model[2] yields time constants of 6.5±0.2 ps for the TA data recorded at λ_{exc} = 490 nm and 5.6±0.2 ps for the TA data at λ_{exc} = 515 nm. This model combines ILET and vibrational cooling as $^3MLCT_{dpph} \rightarrow {}^3MLCT_{tpy}$ inter-ligand internal conversion. The evolution associated spectra obtained from the global analysis are shown in Figure 6a.

Displayed in Figures 5a and 5c are the TA spectra and kinetic traces of **$RuPt_{dpph}$** following excitation at 490 nm, and analogous data obtained following 525 nm excitation are presented in Figures 5b and 5d. Data recorded at 515 nm excitation are provided in Section 3 of the Supporting Information. The spectrotemporal features are qualitatively analogous to **Ru_{dpph}**. In addition to Ru-based transitions, Ru/Pt complexes are also known for Pt-based MLCT transitions, in particular in the range between 300-420 nm.[25] The absence of a significant effect of the Pt moiety on the GSB at early timescales suggests that for **$RuPt_{dpph}$** Ru-based transitions are dominant at the excitation wavelengths used.

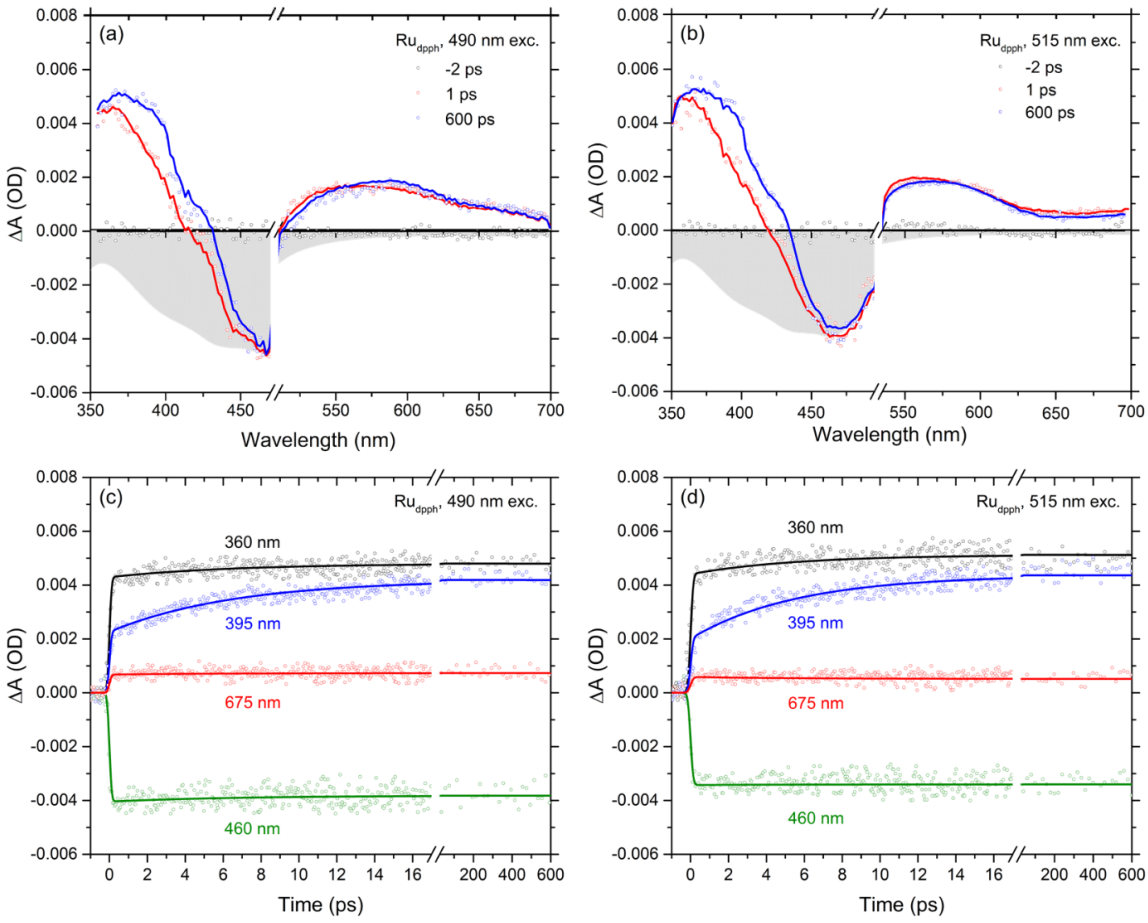

Figure 4. TA spectra at various time delays for **Ru_{dpph}** in anhydrous acetonitrile for excitation at (a) 490 nm and (b) 515 nm. The grey area represents the scaled and inverted steady-state absorbance spectrum. Kinetic traces at key probe wavelengths are shown in (c) following excitation at 490 nm and (d) following excitation at 515 nm. The solid lines in Figs. a-d present a fit from global analysis based on a one-component sequential model.[2]

The ESA band in the UV region likely due to ligand-centered transions of the reduced dpph ligands is redshifted to *ca.* 360 nm compared to **Ru$_{dpph}$**. The broad ESA band around 420 nm likely associated with ligand-centered transitions of the reduced tpy ligand is less intense and changes less in time, possibly due to delocalisation of electron density over the tpy ligand and the catalyst unit (see below). This ESA band may also be redshifted and/or broadened, explaining the *ca.* 5 ps component in the kinetic traces at 460 nm dominated by GSB. Global analysis of all TA data using a one-component sequential model[2] combining ILET and vibrational cooling as inter-ligand internal conversion gives time constants of 4.9±0.2 ps for λ_{exc} = 490 nm, 5.6±0.3 ps for λ_{exc} = 515 nm and 12.3±0.8 ps for λ_{exc} = 525 nm, likely reflecting internal conversion from the dpph ligands to the tpy bridging ligand and/or the catalytic moiety. The longer time constant for inter-ligand internal conversion in particular for λ_{exc} = 525 nm relative to λ_{exc} = 490 nm is clearly illustrated by the comparison of the ESA signals at 360 nm (Fig. 5c *vs* Fig. 5d). The evolution associated spectra obtained from global analysis are shown in Figure 6b. It appears that the internal conversion time constant increases with decreasing photoexcitation energy, which indicates that the energy barrier for ILET increases with vibrational cooling (see Fig. 7). The ESA band around 360 nm associated with the populated ^{3}MLCT$_{dpph}$ states is still present after inter-ligand internal conversion, albeit with lower intensity, indicating that the internal conversion quantum yield is less than unity.

The evolution associated spectra obtained from global analysis of all TA data shown in Figure 6 summarise the role of the photoexcitation energy for **Ru$_{dpph}$** (a) and **RuPt$_{dpph}$** (b). EAS1 characterises the TA spectra before inter-ligand internal conversion and EAS2 is representative of the population of excited states afterwards. The EAS spectra for **Ru$_{dpph}$** indicate a minor role of the photoexcitation energy, with a change in shape of the broad ESA band >500 nm possibly related to the reduced tpy[8b] and dpph[11b] ligands. Hence, the population of excited states in **Ru$_{dpph}$** is possibly not equilibrated, unlike the observation of a Boltzmann distributed population of the ^{3}MLCT states in *ca.* 100 ps independent of the excitation wavelength (for a comparison of 400 nm and 480 nm) for related heteroleptic Ru^{II}-complexes.[11b] The EAS for **RuPt$_{dpph}$** (Fig. 6b) also depend on the excitation wavelength, indicating the absence of an excited state equilibrium. Increasing the excitation wavelength leads to a decrease in amplitude of the ESA band around 360 nm likely associated with populated ^{3}MLCT$_{dpph}$ states. Also the broad ESA band >500 nm becomes more intense, both before internal conversion (EAS1) and afterwards (EAS2). This effect is unlikely due to an increase in population of the ^{3}MLCT$_{tpy}$ states with excitation wavelength, as an increase in signal around 420 nm is absent.

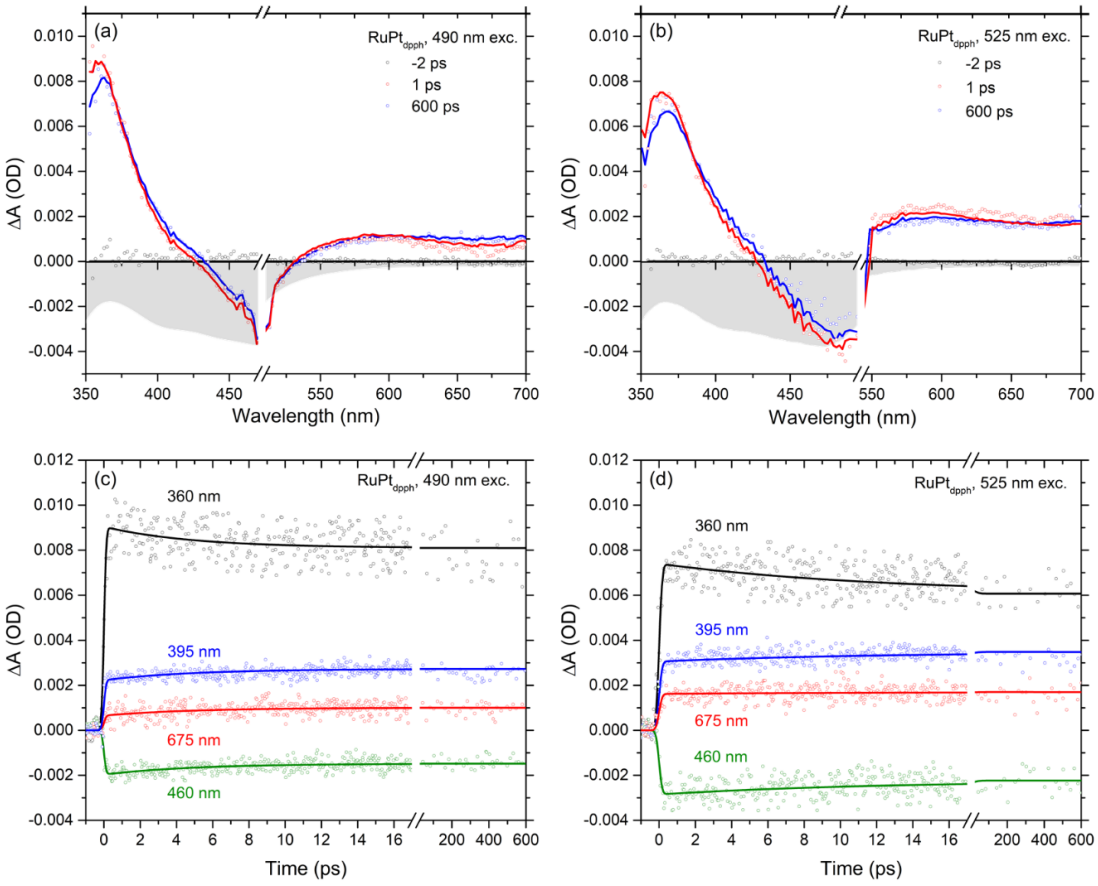

Figure 5. TA spectra at various time delays for **RuPt$_{dpph}$** in anhydrous acetonitrile for excitation at (a) 490 nm and (b) 525 nm. The grey area represents the scaled and inverted steady-state absorbance spectrum. Kinetic traces at key probe wavelengths are shown in (c) following excitation at 490 nm and (d) following excitation at 525 nm. The solid lines in Figs. a-d present a fit from global analysis based on a one-component sequential model.[2]

Table 2. Time constants obtained from global analysis using a one-component sequential model[2] combining ILET and vibrational cooling as inter-ligand internal conversion.

Excitation wavelength	490 nm	515 nm	525 nm
Ru_{dpph}	6.5±0.2 ps	5.6±0.2 ps	
$RuPt_{dpph}$	4.9±0.2 ps	5.6±0.3 ps	12.3±0.8 ps

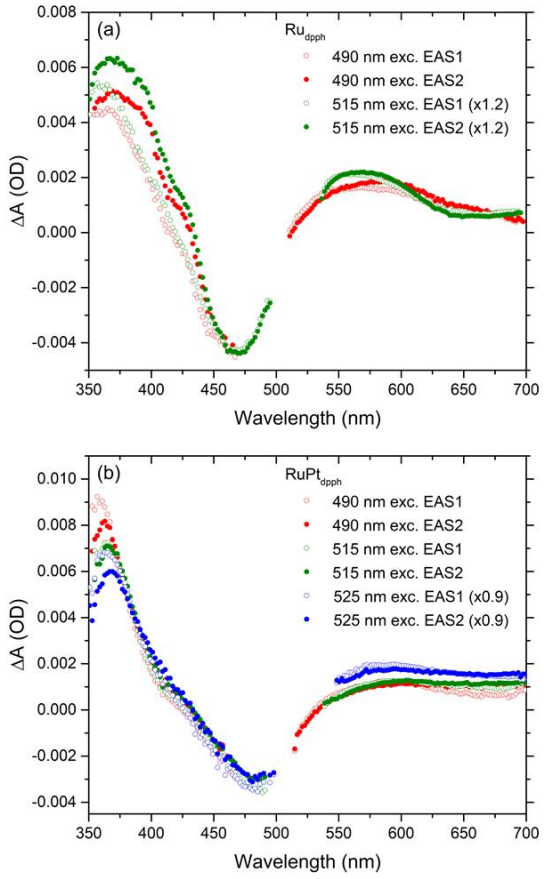

Figure 6. Evolution associated spectra (EAS) for **Ru_{dpph}** (a) and **$RuPt_{dpph}$** (b) for excitation at various wavelengths. EAS1 is representative of the TA spectra prior to inter-ligand internal conversion and EAS2 describes the TA spectra afterwards. A number of EAS spectra have been scaled by the factor indicated in the legend to achieve similar GSB intensities.

An equivalent increase in ESA signal above *ca.* 530 nm for **$RuPt_{bpy}$** has been assigned to an increase in population of a tpy-Pt-I delocalised T_3 state.[20] A similar effect explains the excitation wavelength dependence here, although the nature of the T_3 state in **$RuPt_{dpph}$** may be different. Also the associated dynamics are different. The T_3 state in **$RuPt_{bpy}$** quenches the ^{3}MLCT states on a ~1 ps timescale.[20] In **$RuPt_{dpph}$** the T_3 state is most likely populated within the instrumental response time of *ca.* 100 fs, as the associated increase in signal >500 nm in particular for excitation at 525 nm is already present in EAS1. Also the ~100 ps process found for **$RuPt_{bpy}$** cautiously assigned to electron density redistribution over the tpy-Pt-I moiety[20] is not observed for **$RuPt_{dpph}$**.

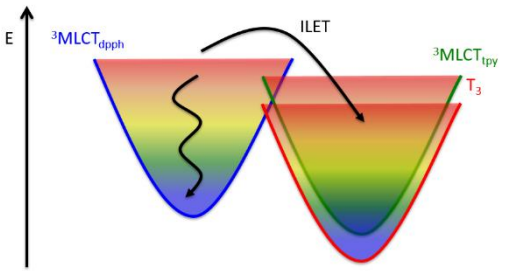

Figure 7. Photophysical model of the processes in **$RuPt_{dpph}$** following ultrafast intersystem crossing into the triplet manifold. For simplicity the singlet potential energy surfaces and the ground state are not shown. The time values for internal conversion are likely determined by the competition between inter-ligand electron transfer (ILET) and vibrational relaxation, and are hence photoexcitation wavelength dependent (see Table 2).

Figure 7 presents a photophysical model for **$RuPt_{dpph}$**. Ultrafast (<100 fs[4b, 4c, 23]) intersystem crossing leads to population of both the ^{3}MLCT$_{dpph}$ and the ^{3}MLCT$_{tpy}$ states, in addition to a further state referred to as T_3 state, likely with triplet character. As lowering the photoexcitation energy most likely results in enhanced population of the T_3 state and a lower population of ^{3}MLCT$_{dpph}$ states, the first is likely lower in energy, explaining the directionality of ILET. The non-equilibrated population of the excited states likely originates from a relatively high energy barrier for ILET and the involvement of vibrational cooling. In fact, vibrational cooling which typically occurs in 5-15 ps[8b, 10] likely competes with ILET, implying an increase in energy barrier in time[11b] and causing a part of the electron density to relax at the peripheral dpph ligands. This non-equilibrated population of excited states is seemingly in contradiction to the mono-exponential photoluminescence decay observed for **$RuPt_{dpph}$** (Fig. 2b), as one can expect the number of non-equilibrated emitting excited states to be reflected by the order of the exponential decay.[8b, 26] One possible explanation is that the populated excited states have comparable lifetimes. A second possibility is that the photoluminescence is dominated by either ^{3}MLCT$_{dpph}$ states or ^{3}MLCT$_{tpy}$/T_3 states. The latter scenario is most likely, as the ns transient absorption data (see Section 4 of the Supporting Information) are well described by a two-component parallel decay model with decay times of 219±5 ns and 650±9 ns. The latter value is in the same order of magnitude as the 795±8 ns photoluminescence lifetime (Fig. 2b).

The initial H_2 TOF of **$RuPt_{dpph}$** exceeds the value obtained for **$RuPt_{bpy}$**. This improvement may be due to an extended excited state lifetime (Table 1). **$RuPt_{dpph}$** however shows a lower initial H_2 TOF than **$RuPt_{dceb}$**. A key difference between these two complexes is the presence/absence of an excited state equilibrium. The high photocatalytic H_2 activity for **$RuPt_{dceb}$** is likely either due to i) an effect of the electron storage position localised at the peripheral ligands on accumulative charge separation and/or ii) an excited state equilibrium allowing electrons to move from the electron reservoir to the catalyst.[12] Although H_2 formation relies on the interplay of various photodynamical processes occuring at different timescales, the absence of an excited state equilibrium in **$RuPt_{dpph}$** deduced from this work may have important consequences and explain the lower initial H_2 TOF value observed for **$RuPt_{dpph}$** relative to **$RuPt_{dceb}$**. This study hence suggests that the mechanism behind

the beneficial effect of using long-lived excited states localised at peripheral ligands as the electron storage reservoir is related to an excited state equilibrium rather than to accumulative charge separation. Realising stable dpph-based Ru/Pt photocatalysts showing an excited state equilibrium hence shows promise to further increase the performance of Ru/Pt and analogous supramolecular photocatalysts.

Conclusions

We have designed a novel Ru/Pt photocatalyst based on dpph peripheral ligands and studied the photodynamical and H_2 generating ability. After photoexcitation and ultrafast intersystem crossing, both triplet excited states localised on the peripheral dpph ligands and states on the bridging ligand/Pt moiety become populated in a non-equilibrated way. The absence of an excited state equilibruim may explain the modest photocatalytic H_2 activity observed. The combination of long-lived excited states with an excited state equilibrium holds promise to further increase the H_2 generation ability of this class of complexes.

Experimental Section

Extensive experimental details are provided in the Supporting Information. Section 1 describes the synthesis and characterisation of the complexes. The H_2 evolution experiments are described in Section 2.

Steady-state UV-vis absorbance spectra were recorded using a Shimadzu UV-1800 spectrophotometer. Steady-state photoluminescence spectra were measured by excitation at 480 nm using a Horiba JobinYvon FluoroMax-4 spectrofluorometer. Both UV-vis absorbance and photoluminescence spectra were recorded at room temperature.

Time-resolved photoluminescence and ns TA data were recorded using an Edinburgh Instruments LP980 Transient Absorption Spectrometer. The samples were prepared in anhydrous acetonitrile (Sigma-Aldrich, purity >99.9 %) and degassed by 3 cycles of freeze-pump-thaw. The samples had a typical absorbance (in optical density OD) at the excitation wavelength (355 nm) equal to 0.31-0.36.

The fs TA setup consists of an amplified Ti:Sa system (Coherent, Legend Elite), which produces 800 nm laser pulses at 5 kHz repetition rate. Part of this 800 nm output was directed into an optical parametric amplifier (Coherent, Opera) to generate the 490 nm, 515 nm or 525 nm pump beam used for photoexcitation. A fraction of the remaining part of the fundamental 800 nm beam was guided through a delay stage and focused onto a CaF_2 crystal (Newlight Photonics, 3 mm thickness) to generate a broadband white light continuum probe extending into the UV till *ca.* 350-360 nm. The CaF_2 crystal was mounted on a continuously moving stage to avoid thermal damage. The remaining 800 nm fundamental was removed by using two 700 nm short pass filters. The polarisations of the pump and probe beams were set at 54.7° to avoid anisotropy effects. The pump was focused to a spot of *ca.* 250 μm diameter, significantly larger than the focused probe spot (*ca.* 100 μm diameter) and it is thus reasonable to assume a homogenously excited sample. The probe pulses were sent into a 15 cm spectrograph coupled to a home built 256 pixels diode array detector. The differential absorbance between pump on and off was determined by chopping the pump beam at 2.5 kHz. The time resolution is *ca.* 100-150 fs.

Samples for fs TA were prepared by dissolving the complexes in anhydrous acetonitrile (Sigma-Aldrich, purity >99.9 %), inserting the sample solution in 1 mm path length quartz cuvettes, followed by bubbling with dry N_2 and sealing. The samples were either excited at 490 nm, at 515 nm or at 525 nm, and had OD values of 0.30, 0.14 and 0.10, respectively. The pump power was kept relatively low ($3\pm1\times10^{14}$ photons/(cm^2 pulse) for λ_{exc} = 490 nm, $5\pm1\times10^{14}$ photons/(cm^2 pulse) for λ_{exc} = 515 nm and $7\pm1\times10^{14}$ photons/(cm^2 pulse) for λ_{exc} = 525 nm) and was verified to be in the linear regime. Samples were checked for photodegradation by comparing UV-vis absorbance spectra before and after the TA measurements and no changes were observed. The TA data were analysed using the open-source program Glotaran.[27] Typical RMS values for the obtained fits are ~$3\cdot10^{-4}$.

Acknowledgements

This work is supported by the Dutch Organisation for Scientific Research (NWO), the EU COST Action CM-1202 (Perspect-H2O, short-term scientific mission 150615-060208), the Sectorplan for Physics and Chemistry and “HYLANTIC”-EAPA 204/2016. LOR thanks the Irish Research Council for a financial support.

Keywords: Ru/Pt photocatalysts • ultrafast photodynamics • inter-ligand internal conversion • excited state equilibrium • electron storage reservoir

[1] J. Barber, *Philos. Trans. Royal Soc. A* **2007**, *365*, 1007-1023.

[2] A one-component sequential model (one fitted time constant τ_1) is based on the following evolution sequence (GS = ground state): $A \xrightarrow{\tau_1} B \rightarrow GS$. In this model species A evolves into species B with time constant τ_1, which is determined from global analysis of the TA data. Species B returns to the GS with a fixed time constant, determined from time-resolved photoluminescence measurements.

[3] a) A. J. Esswein, D. G. Nocera, *Chem. Rev.* **2007**, *107*, 4022-4047;b) M. Martis, K. Mori, K. Kato, G. Sankar, H. Yamashita, *ChemPhysChem* **2013**, *14,* 1122-1125; c) T. J. Meyer, *Nature* **2008**, *451*, 778-779; d) V. Balzani, A. Credi, M. Venturi, *Chemsuschem* **2008**, *1*, 26-58; e) A. Magnuson, M. Anderlund, O. Johansson, P. Lindblad, R. Lomoth, T. Polivka, S. Ott, K. Stensjo, S. Styring, V. Sundstrom, L. Hammarstrom, *Acc. Chem. Res.* **2009**, *42*, 1899-1909; f) Y. Tachibana, L. Vayssieres, J. R. Durrant, *Nat. Photonics* **2012**, *6*, 511-518.

[4] a) A. Juris, V. Balzani, F. Barigelletti, S. Campagna, P. Belser, A. Vonzelewsky, *Coordin. Chem. Rev.* **1988**, *84*, 85-277; b) A. T. Yeh, C. V. Shank, J. K. McCusker, *Science* **2000**, *289*, 935-938; c) A. Cannizzo, F. van Mourik, W. Gawelda, G. Zgrablic, C. Bressler, M. Chergui, *Angew. Chem. Int. Ed.* **2006**, *45*, 3174-3176; d) S. Campagna, F. Puntoriero, F. Nastasi, G. Bergamini, V. Balzani, *Top. Curr. Chem.* **2007**, *280*, 117-214.

[5] a) H. Ozawa, M. A. Haga, K. Sakai, *J. Am. Chem. Soc.* **2006**, *128*, 4926-4927; b) S. Rau, B. Schafer, D. Gleich, E. Anders, M. Rudolph, M. Friedrich, H. Gorls, W. Henry, J. G. Vos, *Angew. Chem. Int. Ed.* **2006**, *45*, 6215-6218; c) C. G. Morales-Guio, L. A. Stern, X. L. Hu, *Chem. Soc. Rev* **2014**, *43*, 6555-6569.

[6] M. Karnahl, C. Kuhnt, F. Ma, A. Yartsev, M. Schmitt, B. Dietzek, S. Rau, J. Popp, *Chemphyschem* **2011**, *12*, 2101-2109.

[7] a) G. S. Bindra, M. Schulz, A. Paul, R. Groarke, S. Soman, J. L. Inglis, W. R. Browne, M. G. Pfeffer, S. Rau, B. J. MacLean, M. T. Pryce, J. G. Vos, *Dalton Trans.* **2012**, *41*, 13050-13059; b) G. S. Bindra, M. Schulz, A. Paul, S. Soman, R. Groarke, J. Inglis, M. T. Pryce, W. R. Browne, S. Rau, B. J. Maclean, J. G. Vos, *Dalton Trans.* **2011**, *40*, 10812-10814; c) M. G. Pfeffer, B. Schafer, G. Smolentsev, J. Uhlig, E. Nazarenko, J. Guthmuller, C. Kuhnt, M. Wachtler, B. Dietzek, V. Sundstrom, S. Rau, *Angew. Chem. Int. Ed.* **2015**, *54*, 5044-5048; d) M. G. Pfeffer, T. Kowacs, M. Wachtler, J. Guthmuller, B. Dietzek, J. G. Vos, S. Rau, *Angew. Chem. Int. Ed.* **2015**, *54*, 6627-6631; e) J. D. Knoll, S. H. Higgins, T. A. White, K. J. Brewer, *Inorg. Chem.* **2013**, *52*, 9749-9760.

[8] a) T. Kowacs, Q. Pan, P. Lang, L. O'Reilly, S. Rau, W. R. Browne, M. T. Pryce, A. Huijser, J. G. Vos, *Faraday Discuss.* **2015**, *185*, 143-170; b) Q. Pan, F. Mecozzi, J. P. Korterik, D. Sharma, J. L. Herek, J. G. Vos, W. R. Browne, A. Huijser, *J. Phys. Chem. C* **2014**, *118*, 20799-20806.

[9] S. Tschierlei, M. Karnahl, M. Presselt, B. Dietzek, J. Guthmuller, L. Gonzalez, M. Schmitt, S. Rau, J. Popp, *Angew. Chem. Int. Ed.* **2010**, *49*, 3981-3984.

[10] a) W. Henry, C. G. Coates, C. Brady, K. L. Ronayne, P. Matousek, M. Towrie, S. W. Botchway, A. W. Parker, J. G. Vos, W. R. Browne, J. J. McGarvey, *J. Phys. Chem. A* **2008**, *112*, 10703-10704; b) S. Wallin, J. Davidsson, J. Modin, L. Hammarstrom, *J. Phys. Chem. A* **2005**, *109*, 4697-4704; c) N. H. Damrauer, J. K. McCusker, *J. Phys. Chem. A* **1999**, *103*, 8440-8446; d) J. Schindler, S. Kupfer, M. Wächtler, J. Guthmuller, S. Rau and B. Dietzek, *ChemPhysChem* **2015**, *16*, 1061-1070.

[11] a) G. Benko, J. Kallioinen, P. Myllyperkio, F. Trif, J. E. I. Korppi-Tommola, A. P. Yartsev, V. Sundstrom, *J. Phys. Chem. B* **2004**, *108*, 2862-2867; b) C. W. Stark, W. J. Schreier, J. Lucon, E. Edwards, T. Douglas, B. Kohler, *J. Phys. Chem. A* **2015**, *119*, 4813-4824; c) C. V. Suneesh, B. Balan, H. Ozawa, Y. Nakamura, T. Katayama, M. Muramatsu, Y. Nagasawa, H. Miyasaka, K. Sakai, *Phys. Chem. Chem. Phys.* **2014**, *16*, 1607-1616.

[12] M. L. A. Abrahamsson, H. B. Baudin, A. Tran, C. Philouze, K. E. Berg, M. K. Raymond-Johansson, L. C. Sun, B. Akermark, S. Styring, L. Hammarstrom, *Inorg. Chem.* **2002**, *41*, 1534-1544.

[13] Q. Pan, L. Freitag, T. Kowacs, J. C. Falgenhauer, J. P. Korterik, D. Schlettwein, W. R. Browne, M. T. Pryce, S. Rau, L. Gonzalez, J. G. Vos, A. Huijser, *Chem. Commun.* **2016**, *52*, 9371-9374.

[14] T. Kowacs, L. O'Reilly, Q. Pan, A. Huijser, P. Lang, S. Rau, W. R. Browne, M. T. Pryce, J. G. Vos, *Inorg. Chem.* **2016**, *55*, 2685-2690.

[15] T. A. White, J. D. Knoll, M. Arachchige, K. J. Brewer, *Materials* **2011**, *5*, 27-46.

[16] L. Hammarstrom, *Acc. Chem. Res.* **2015**, *48*, 840-850.

[17] L. Zedler, J. Guthmuller, I. R. de Moraes, S. Kupfer, S. Krieck, M. Schmitt, J. Popp, S. Rau, B. Dietzek, *Chem. Commun.* **2014**, *50*, 5227-5229.

[18] a) P. C. Alford, M. J. Cook, A. P. Lewis, G. S. G. Mcauliffe, V. Skarda, A. J. Thomson, J. L. Glasper, D. J. Robbins, *J. Chem. Soc. Perk. T. 2* **1985**, 705-709; b) K. F. Mongey, J. G. Vos, B. D. MacCraith, C. M. McDonagh, C. Coates, J. J. McGarvey, *J. Mater. Chem.* **1997**, *7*, 1473-1479.

[19] H. Ozawa, K. Sakai, *Chem. Commun.* **2011**, *47*, 2227-2242.

[20] Q. Pan, F. Mecozzi, J. P. Korterik, J. G. Vos, W. R. Browne, A. Huijser, *Chemphyschem* **2016**, *17*, 2654-2659.

[21] S. Tschierlei, M. Presselt, C. Kuhnt, A. Yartsev, T. Pascher, V. Sundstrom, M. Karnahl, M. Schwalbe, B. Schafer, S. Rau, M. Schmitt, B. Dietzek, J. Popp, *Chem-Eur J.* **2009**, *15*, 7678-7688.

[22] R. Narayana-Prabhu, R. H. Schmehl, *Inorg. Chem.* **2006**, *45*, 4319-4321.

[23] J. K. McCusker, *Acc. Chem. Res.* **2003**, *36*, 876-887.

[24] M. Kovacs, K. L. Ronayne, W. R. Browne, W. Henry, J. G. Vos, J. J. McGarvey, A. Horvath, *Photochem. Photobio. Sci.* **2007**, *6*, 444-453.

[25] M. Kobayashi, S. Masaoka, K. Sakai, *Photochem. Photobio. Sci.* **2009**, *8*, 196-203.

[26] a) E. C. Glazer, D. Magde, Y. Tor, *J. Am. Chem. Soc.* **2007**, *129*, 8544-8551; b) D. Magde, M. D. Magde, E. C. Glazer, *Coordin. Chem. Rev.* **2016**, *306*, 447-467.

[27] J. J. Snellenburg, S. P. Laptenok, R. Seger, K. M. Mullen, I. H. M. van Stokkum, *J Stat Softw* **2012**, *49*, 1-22.

10.1002/cphc.201800658

WILEY-VCH

ARTICLE

Hydrogen generating Ru/Pt bimetallic photocatalysts based on phenyl-phenanthroline peripheral ligands

Laura O'Reilly, Qing Pan, Nivedita Das, Kasper Wenderich, Jeroen P. Korterik, Johannes G. Vos, Mary T. Pryce and Annemarie Huijser**

Present study on a novel supramolecular bimetallic photocatalyst based on dpph peripheral ligands suggests that the realisation of an excited state equilibrium is a key factor to increase the hydrogen generation activity of this class of complexes.

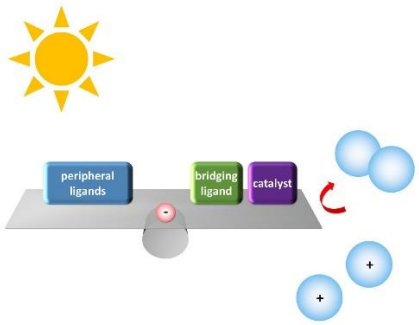

Page No. – Page No.
Hydrogen generating Ru/Pt bimetallic photocatalysts based on phenyl-phenanthroline peripheral ligands